THE ASTROPHYSICAL JOURNAL, 459:L49–L52, 1996 March 10

LOOKING FOR THE SUNYAEV-ZELDOVICH EFFECT TOWARD DISTANT *ROSAT* CLUSTERS OF GALAXIES[1]

P. ANDREANI,[2] L. PIZZO,[3] G. DALL'OGLIO,[4] N. WHYBORN,[5] H. BÖHRINGER,[6] P. SHAVER,[7]
R. LEMKE,[8] A. OTÀROLA,[8] L.-Å. NYMAN,[8] AND R. BOOTH[9]
Received 1995 August 1; accepted 1996 January 3

ABSTRACT

We report on observations of the Sunyaev-Zeldovich effect toward X-ray *ROSAT* clusters taken with a double-channel (1.2 and 2 mm) photometer installed at the focus of the 15 m Swedish ESO Submillimeter Telescope antenna in Chile. This paper describes the first results obtained for the high-z clusters S1077, A2744, and S295. Marginal detections were found for A2744, and at 1 mm for S1077. We discuss these data in terms of contamination of sources along the line of sight and give a constraint on the amplitude of the kinematic effect.

Subject heading: cosmic microwave background

1. INTRODUCTION

The Sunyaev-Zeldovich (SZ) effect is a characteristic signature on the cosmic microwave background (CMB) radiation spectrum originated from (inverse) Compton scattering of the photons by hot electrons in clusters of galaxies. There has been considerable interest in its detection because of its potential as a diagnostic tool for observational cosmology (physical process in the earlier universe; determination of H_0 and q_0 and peculiar velocities of clusters) and for the study of the intracluster medium (see the original papers by Zeldovich & Sunyaev 1969; Sunyaev & Zeldovich 1972, 1981). Its detection has been the goal of many observational searches (e.g., Birkinshaw 1990), mostly in the Rayleigh-Jeans (RJ) part of the spectrum, where the scattering leads to an intensity decrement. However, interpretation of measurements in the RJ side is plagued both by the possible radio emission from sources within the clusters and by the smallness of the effect. After many attempts to detect this effect (see, e.g., the review paper by Birkinshaw 1990), radio observations show the expected decrement at centimeter wavelengths toward A2218, A665, 0016+16, A773, and Coma (Birkinshaw 1991; Klein et al. 1991; Jones et al. 1993; Grainge et al. 1993; Herbig et al. 1995) and at 2.2 mm toward A2163 (Wilbanks et al. 1994).

Measurements near the Planckian peak and on the Wien side are in principle more attractive, since (*a*) the intensity enhancement relative to the Planckian value is larger than the magnitude of the RJ decrement; (*b*) the simultaneous detection of the enhancement (positive) and decrement (negative) on the same cluster provides an unambiguous signature of their presence; (*c*) sources in the cluster are expected to give a negligible contribution at high frequency; and (*d*) because of the large bandwidth, the sensitivity of bolometer systems is excellent.

We have built a photometer with two bolometers centered at 1.2 and 2 mm to feed the Osservatorio Antartico Submillimetrico Infrarosso (OASI) telescope installed at the Italian base in Antarctica (Dall'Oglio et al. 1992). This photometer was adapted to the focus of the Swedish ESO Submillimeter Telescope (SEST), and its performances were tested during an observing run in 1994 September. Most of the allocated time was spent in installing the photometer and testing the equipment (Pizzo et al. 1995a), but some useful observations were gathered toward S1077, A2744, and S295.

2. THE INSTRUMENT

The instrument was described in detail elsewhere (Pizzo et al. 1995a); here only the main characteristics are summarized. The photometer uses two Si bolometers cooled to 0.3 K by means of a single-stage ^{3}He refrigerator (Pizzo, Martinis, & Dall'Oglio 1995b). Radiation coming from the telescope is focused by a PTFE lens and enters the cryostat through a polyethylene vacuum window and two cooled filters. A dichroic mirror (beam splitter) at 4.2 K divides the incoming radiation between two f/4.3 Winston cones cooled at 0.3 K and located orthogonal to each other. The wavelength ranges are defined by two interference filters centered at 1.2 and 2 mm and cooled at 4.2 K, with bandwidth 350 and 560 μm, respectively. The 2 mm band includes the peak brightness of the decrement in the SZ thermal effect, while the 1.2 mm bandwidth is a compromise between the maximum value of the enhancement in the SZ and the atmospheric transmission.

Since our goal is the simultaneous observation of the same source region, comparable beam sizes at the two different frequencies were achieved using Winston cones with the same entrance sizes for both channels, selected to have roughly a diffraction-limited configuration for the 2 mm channel. Beam shape and dimension were measured using raster scans on Saturn, Jupiter, and Uranus (details on the procedure used and on the map reconstruction are in Haslam 1974, Sievers et al. 1991, and Lemke 1992). The planet maps show a good alignment (within 2″) of the two beams and their symmetry around the optical axis. Their half-power beamwidths turn out to be 44″ (1.2 mm channel) and 46″ (2 mm channel).

Since clusters of galaxies are extended sources, in order to have the reference beam as far as possible from the peak

[1] Based on observations collected with the ESO-Swedish SEST 15 m telescope (La Silla, Chile).

[2] Dipartimento di Astronomia, Vicolo Osservatorio 5, I-35122, Padua, Italy, andreani@astrpd.pd.astro.it; and European Southern Observatory, Garching, Germany, pandrean@eso.org.

[3] Istituto TESRE, C.N.R., via P. Gobetti, Bologna, Italy; pizzo@botes1.bo.astro.it.

[4] Dipartimento di Fisica, III Univ. Roma, P.le Aldo Moro 2, I-00185 Rome, Italy; dalloglio@roma1.infn.it.

[5] SRON, Groningen, P.O. Box 800, Groningen, Netherlands; nick@sron.rug.nl.

[6] Max-Planck-Institut für extraterrestrische Physik, Garching, Germany.

[7] European Southern Observatory, Garching, Germany; pshaver@eso.org.

[8] European Southern Observatory, La Silla, Chile; rlemke, aotarola, lnyman@eso.org.

[9] ONSALA Space Observatory, Onsala, Sweden.

TABLE 1

X-RAY PROPERTIES AND FINAL VALUES

ROSAT CLUSTER			$(\Delta T)_{\rm therm}$		COMPTONIZATION
Name	Redshift	L_X(0.1–2.4 keV) (10^{45} ergs s^{-1})	1 mm (mK)	2 mm (mK)	PARAMETER (10^{-4})
S1077	0.312	0.66 ± 0.16	0.9 ± 0.3	−0.8 ± 0.5	5.3 ± 1.8
A2744	0.308	2.00 ± 0.05	0.8 ± 0.3	−1.4 ± 0.4	3.8 ± 1.2
S295	0.299	1.30 ± 0.15	0.1 ± 0.3	−2.5 ± 1.0	<5.3 (3 σ)

region of the X-ray emission, the chop throw was set to the maximum possible amplitude, i.e., that corresponding to a beam separation on the sky of 135″. The coupling between the antenna and the photometer was checked by comparing the output signals from known sources at the 1.2 mm channel of our photometer with those at the 1.2 mm MPI bolometer available at SEST (Kreysa 1990), both having a filter very similar in transmission and shape. Taking into account the correction factors due to the different fields of view, equal signals within the error bars have been found.

The detector noise of both channels measured at the focus was about 50 nV Hz$^{-1/2}$. Responsivities were inferred with Venus, Saturn, Uranus, Mars, and Jupiter taking the planet brightness temperatures from Ulich (1981) and Ulich et al. (1984): the effective responsivities at the focus turned out to be 1.8 and 0.7 μV K^{-1} at 1.2 and 2 mm, respectively. This means that the measured values for the noise equivalent power were 28 and 70 mK Hz$^{-1/2}$, i.e., 14 and 35 mK in 1 s integration time. The average uncertainty on these figures is 10%. Converting these values in thermodynamic temperatures gives for the measured sensitivities $\Delta T/T = 0.014$ and $\Delta T/T = 0.02$ at 1.2 and 2 mm, respectively (1 s integration time).

Atmospheric transmission was monitored by frequent sky-dips, i.e., telescope scans at constant azimuth and different elevation are carried out to compare the atmospheric emission with that of an absorber moved into the path of the reference beam. The position of the sources was found by first pointing a nearby radio-loud quasar with strong millimetric fluxes and then pointing the X-ray coordinates. With this procedure, we reduce the pointing errors to less than 2″.

3. THE OBSERVING STRATEGY

Targets were selected for their high X-ray luminosities in the *ROSAT* band (0.1–2.4 keV). They are extended X-ray sources identified as optical high-redshift ($z \sim 0.3$) clusters. Names, redshifts, and *ROSAT* luminosities are listed in Table 1. If we assume a core radius of 250–400 kpc in standard cosmologies, their apparent size is 45″–70″; a chop throw of 135″ means that, at the reference beam position, the ratio between the electron density, $n_e(\theta = 135'')$, and its central value, $n_e(\theta = 0)$, is ~0.28–0.42, i.e., we lose 30%–40% of the signal because of the limited chop throw. The effective values of y, taking account of the SZ effect in the off-center positions, can be roughly estimated only for A2744, for which a deep Position Sensitive Proportional Counter exposure is already available.[10] The gas density was derived from the best-fit value of a β-model to the surface density profile, and the temperature was assumed to be 7 keV; y turns out to be 1.3×10^{-4}. For S1077 and S295, the X-ray properties listed in Table 1 were taken from the *ROSAT* All-Sky Survey and the luminosities were estimated assuming $T_e = 7$ keV.

We have checked that the selected candidates do not contain IR sources of the *IRAS* Faint Source Catalog (Moshir et al. 1989), but sources fainter than the 90% completeness limit of this survey (~230 mJy at 60 μm) may fall in our beam. On the basis of our observations on galaxies performed at SEST and IRAM (Andreani & Franceschini 1992; Franceschini & Andreani 1995), the expected millimetric emission, scaled at the cluster redshift, is less than 0.8 mJy at 1.2 mm. This flux would produce an output signal in antenna temperature of 0.03 mK, which is lower than the expected signals from the SZ effect (see below).

The magnitude of the expected signals from the effect was estimated by convolving $\Delta T/T = y[x(e^x + 1)/(e^x - 1) - 4]$ with the spectral filter response, the atmospheric transmission, and the beam shape, where T is the CMB temperature, $x = h\nu/kT$, and $y = \int (kT_e/mc^2) n_e \sigma_T \, dl$ is the Comptonization parameter, n_e, T_e being the electron density and temperature. We find $\Delta T/T \sim 0.69y$, $\Delta T/T \sim -1.77y$ at 1.2 and 2 mm, respectively, for the thermodynamic temperatures.

In order to reduce the atmospheric noise and systematics from the antenna, two combined observing strategies were exploited.

1. To reduce temporal and spatial drifts of the atmosphere, a three beams technique (beam switching plus nodding) was applied. We call position A the source in the right beam with the reference beam on the left and position B the source in the left beam with the reference beam on the right. The antenna tracks each position to integrate 10 s and moves according to the following temporal sequence: ABBAABBAA . . . A. Twenty positions are tracked so that the entire cycle lasts 200 s, which is the shortest integration time and, in the following, will be called one scan (see § 4 for further details). The duty cycle was 80%, i.e., additional 4 s are spent for each movement of the antenna between positions A and B.

2. In order to properly quantify the contribution to the source signals from unknown systematics, we measured them using the following procedure. Each source was integrated over time chunks of 600 s (three of the above scans); this time interval plus the needed overheads give a total tracking time on the source of 15 minutes. The same time was spent on a blank sky located in equatorial coordinates 15 minutes ahead in right ascension. This means that the antenna tracks twice the same sky position in horizontal coordinates: once ON the source and the other OFF the source. This enables us to compare the two different measurements and quantify the spurious signals (atmosphere plus antenna systematics). The choice of 600 s of integration ON and OFF the source is a compromise between the minimization of the time wasted on overheads and the need of minimizing the atmospheric variations between one observation and the other.

[10] *ROSAT* HRI observations are already scheduled for S1077 and S295.

4. DATA ANALYSIS

As described in § 3, the data consist of chunks of three scans, each containing 20 subscans of 10 s corresponding to either position A or position B. The reduction procedure is done in several steps. (1) The data of one scan (200 s: 440 data points) are roughly Gaussian, distributed with a width larger than the detector noise because of the atmospheric noise. In order to get rid of individual data inconsistent with the underlying Gaussian distribution, each datum with a value exceeding 3 times the rms of the entire scan was rejected. This criterion eliminates spikes due to equipment malfunction or sudden atmospheric variation. The fraction of rejected data is 1%. (2) Within each subscan, high-frequency atmospheric noise was filtered with the Savitzky-Golay algorithm (Press & Teukolsky 1990), which smooths the time series within a moving window by approximating the underlying function by a polynomial of second to third order. At each point, the least-squares fit to the $n_L + n_R + 1$ points in the moving window is assigned, where n_L and n_R are the parameters chosen to smooth the data over a bin of $3t_0$ (t_0 being the integration time of the lock-in amplifiers, i.e., twice the inverse of the chopping frequency, 4.4 Hz). A mean value of the differential sky temperature (T_A^a or T_B^a) is then obtained for each subscan, whose variance is found with a procedure of bootstrap resampling (e.g., Barrow, Bhavsar, & Sonoda 1984). This method is widely used to take into account correlation among data (induced in this case by the filtering). (3) The signal is obtained by subtracting each couple of subscans $\Delta T_i^a = (T_A^a - T_B^a)/2$ with variance $2\sigma_i^2 = \sigma_A^2 + \sigma_B^2$. (4) For each 200 s scan, the average value is $\Delta T_m^a = [\Sigma_i(\Delta T_i^a)/\sigma_i^2]/\Sigma_i\sigma_i^{-2}$, with a scatter of $\sigma_m^2 = \Sigma_i(\Delta T_i^a - \Delta_m^a)^2\sigma_i^{-2}/[(\Sigma_i\sigma_i^{-2})(M-1)]$.

The weighted mean over the three scans is (at the sky position P) $\Delta T_P^a = (\Sigma_{m=1}^3 \Delta T_m^a \sigma_m^{-2}/\Sigma_{m=1}^3 \sigma_m^{-2})$, with a scatter about the mean of $\sigma_P^2 = [\Sigma_{m=1}^3(\Delta T_m^a - \Delta T_P^a)^2\sigma_m^{-2}/\Sigma_{m=1}^3\sigma_m^{-2}]$.

For each ΔT_m^a, a weight is assigned: $w_m = (\sigma_m^2 + \sigma_P^2)^{-1}$, where σ_m^2 represents the variance due to short-term fluctuations, and σ_P^2 that due to medium-term variations. The final *weighted* mean, over the sky position P, is given by

$$\langle \Delta T^a \rangle_f = \frac{\sum_{m=1}^{3} \Delta T^a{}_m w_m}{\sum_{m=1}^{3} w_m},$$

with estimated variance

$$\sigma_f^2 = \frac{\sum_{m=1}^{3} (\Delta T^a{}_m - \langle \Delta T^a \rangle_f)^2 w_m}{2\sum_{m=1}^{3} w_m}.$$

Values obtained when the antenna tracked the source for 600 s (three scans), hereafter called signal ON, are subtracted from those taken when the antenna was 15 minutes ahead in R.A. (hereafter called signal OFF),

$$\Delta T^a_{\rm SZ} = (\Delta T_f^a)_{\rm ON} - (\Delta T_f^a)_{\rm OFF},$$

and the quadratic sum of the two standard deviations has been used as error bar, $\sigma^2_{\rm SZ} = (\sigma_f^2)_{\rm ON} + (\sigma_f^2)_{\rm OFF}$. $(\Delta T_f^a)_{\rm ON}$ and $(\Delta T_f^a)_{\rm OFF}$ with their error bars are plotted in Figure 1 for the three clusters and for each channel. The final values, the weighted means over all the subtracted scans in thermodynamic values, and the corresponding y parameters are listed in Table 1.

5. DISCUSSION

The size of the y value of A2744 derived in Table 1 disagrees with the estimated one (see § 3) and cannot be reliably ascribed to the sole SZ thermal effect unless some relevant information is missed in the X-ray data. The resulting data toward A2744 at 1.2 and 2 mm and S1077 at 1.2 mm could therefore be originated from other sources. Here possible contaminations are briefly discussed.

5.1. *Contamination of Kinematic Effect*

Peculiar velocities of clusters could contribute significantly to the signals for values larger than $v_r > 1000$ km s^{-1}. In fact, the ratio between the SZ kinematic effect, $\Delta T/T = (v_r/c)\tau$ (where $\tau = \int \sigma_{\rm T} n\, dl$ is the optical depth for Thomson scattering along the line of sight and v_r is the peculiar velocity), and the thermal effect depends on the cluster's peculiar velocity and the gas temperature. The lack of any other observations of peculiar velocities on these clusters makes the quantification of this contribution impossible, and, on the basis of the present knowledge, we cannot exclude that a fraction of the signals is due to it, even if large peculiar velocities seem quite unlikely in most cosmological scenarios. The present data can be used to constrain the combination $\tau(v_r/c)$, which turns out to be less than 3×10^{-4} for A2744, S1077, and S295 (3 σ values).

5.2. *Contamination of Cluster Sources*

As mentioned in § 3, a strong contamination from sources in the cluster seems to be unlikely: (*a*) clusters do not contain many spirals, (*b*) late-type galaxies at this redshift would have a millimetric emission below the expected signals from the SZ effect, and (*c*) we are looking at the very center of the cluster that, as shown from optical images, is devoid of sources. Only the cluster S295 has three ellipticals very close to the center of the X-ray image, and part of their emission can therefore fall in our beam. If there was a significant nonthermal emission, we would expect to find positive signals in both channels, contrary to our results (see Table 1).

Let us suppose that one or more of the sources fall in one of the reference beams. In this case, if a millimeter emitting source was located in the right beam, we would find a positive signal in both channels. If it was in the left reference beam, the signal would be negative in both channels. This seems to be unlikely since we do not find these systematics (see Table 1). However, contribution from cluster sources deserves further investigations and will be the goal of future projects.

It is also unlikely that both signals are contaminated from the emission of unresolved sources: the estimate of their confusion limit in the beam made by Franceschini et al. (1991) gives at 1.2 mm $\Delta I \sim 0.4$ mJy, i.e., $\Delta T \sim 0.06$ mK.

5.3. *Contamination by Other Spurious Signals*

We have considered other effects affecting the signals: (*a*) The selected clusters have sizes comparable to our beams, and beam dilution cannot significantly lower the detection probability (Rephaeli 1987), but fluxes are reduced up to 30%–40% because of the limited chop throw. (*b*) Diffraction patterns could enter the beams and alter the signals, but constant systematics of this type should be removed by our observing strategy (see § 3). However, if the antenna did not track precisely the same paths relative to the local environment, because of a loss of synchronization, some spurious signals would survive, and we cannot exclude at present that this never

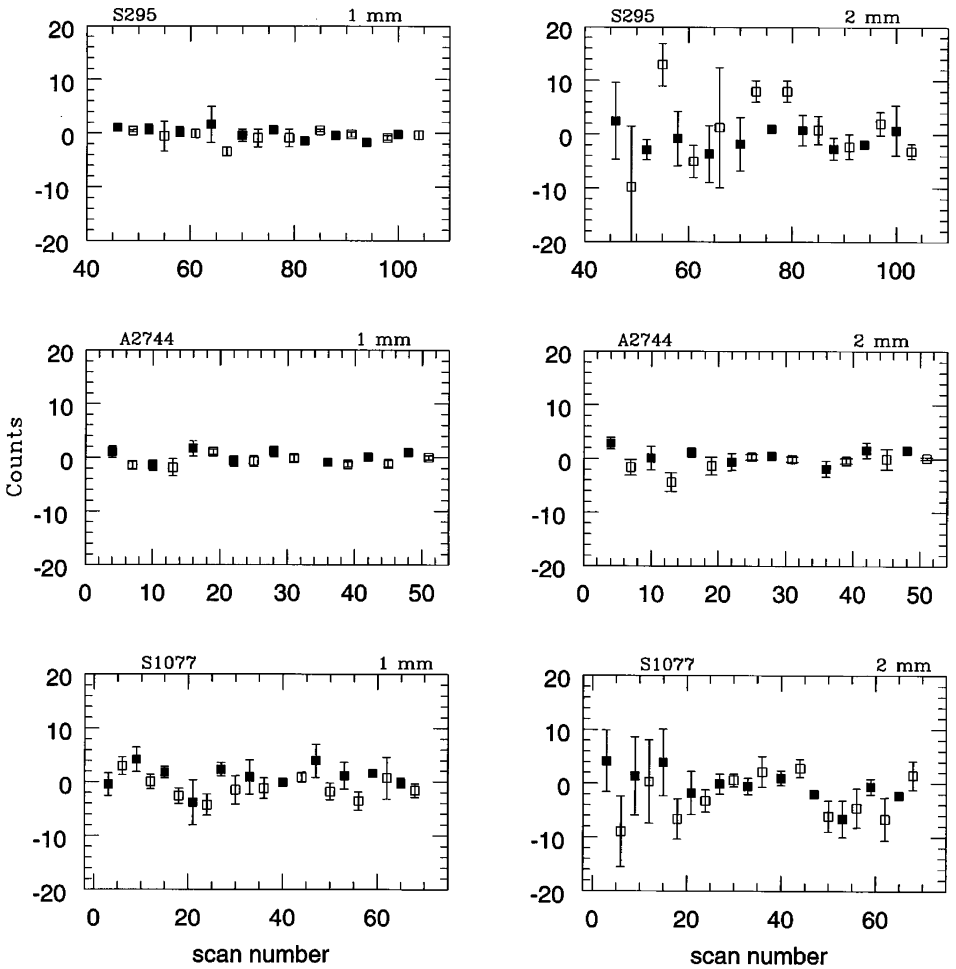

FIG. 1.—Antenna temperature differences for positions OFF (*open squares*) and ON (*filled squares*) the source. Right panels refer to the 2 mm channel, while the left ones refer to the 1 mm channel. Note that in most cases the 2 mm signals ON the sources lie below the corresponding one OFF the sources. The statistical significance, however, is very low. The corresponding panels for the 1 mm channel show the opposite trend, meaning that the signals from the sources are higher than those OFF the sources.

happened. (*c*) We checked if sources were located in the OFF position (15 minutes ahead in R.A.): from the *IRAS* Faint Source Catalog and 5 GHz NRAO survey, it turns out that none fall in these areas. The *IRAS* 100 μm sky maps do not show any emission from galaxy cirrus at a level greater than their zero level.

The authors are indebted to Glenn Persson and to the ESO Workshop team at La Silla. This work has been partially supported by the P.N.R.A. (Programma Nazionale di Ricerche in Antartide) and made use of the *Skyview* Database, developed under NASA ADP grant NAS 5-32068. Very useful comments by an anonymous referee helped to improve this paper.

REFERENCES

Andreani, P., & Franceschini, A. 1992, A&A, 260, 89
Barrow, J. D., Bhavsar, S. P., & Sonoda, D. H. 1984, MNRAS, 210, 19
Birkinshaw, M. 1990, in The Cosmic Microwave Background: 25 Years Later, ed. N. Mandolesi & N. Vittorio (Dordrecht: Kluwer), 77
———. 1991, in Physical Cosmology, ed. A. Blanchard et al. (Gif-sur-Yvette: Editions Frontières), 177
Dall'Oglio, G., et al., 1992, Exp. Astron., 2(5), 256
Franceschini, A., & Andreani, P. 1995, ApJ, 440, L5
Franceschini, A., et al. 1991, A&AS, 89, 285
Grainge, K., et al. 1993, MNRAS, 265, L57
Halsam, C. G. T. 1974, A&AS, 15, 333
Herbig, T., Lawrence, C. R., Readhead, A. C. S., & Gulkis, S. 1995, ApJ, 449, L5
Jones, M., et al. 1993, Nature, 365, 322
Klein, U., Rephaeli, Y., Schlickeiser, R., & Wielebinski, R. 1991, A&A, 244, 43
Kreysa, E. 1990, in From Ground-based to Space-borne Sub-mm Astronomy, ed. J.-P. Swings & D. Fraipont (ESA SP-314) (Noordwijk: ESA), 265
Lemke, R. 1992, Ph.D. thesis, Univ. Bonn
Moshir, M., et al. 1989, Explanatory Supplement to the *IRAS* Faint Source Survey (Pasadena: JPL)
Pizzo, L., Andreani, P., Dall'Oglio, G., Lemke, R., Otàrola, A., & Whyborn, N., 1995a, Exp. Astron., 6, 249
Pizzo, L., Martinis, L., & Dall'Oglio, G. 1995b, preprint
Press, W. H., & Teukolsky, S. A. 1990, Comput. Phys., 4, 669
Rephaeli, Y. 1987, MNRAS, 228, 29
Sievers, A. W., Mezger, P. G., Gordon, M. A., Kreysa, E., Haslam, C. G. T., & Lemke, R. 1991, A&A, 251, 231
Sunyaev, R. A., & Zeldovich, Ya. B. 1972, Comments Astrophys. Space Phys., 4, 173
———. 1981, Ap&SS, 1, 11
Ulich, B. L. 1981, AJ, 86, 1619
Ulich, B. L., et al. 1984, Icarus, 60, 590
Wilbanks, T. M., et al. 1994, ApJ, 427, L75
Zeldovich, Ya. B., & Sunyaev, R. A. 1969, Ap&SS, 4, 301